Aluminum (III) Interactions with the Side Chains of Aromatic Aminoacids

ARTICLE *in* INTERNATIONAL JOURNAL OF QUANTUM CHEMISTRY · JANUARY 2002

Impact Factor: 1.43 · DOI: 10.1002/qua.952

Aluminum (III) Interactions with the Side Chains of Aromatic Aminoacids

JOSE M. MERCERO, JON M. MATXAIN, XABIER LOPEZ, JOSEPH E. FOWLER, JESUS M. UGALDE

Kimika Fakultatea, Euskal Herriko Unibertsitatea, P.K. 1072, 20080 Donostia, Euskaldi, Spain

Received 21 August 2001; accepted 6 March 2002

DOI 10.1002/qua.952

ABSTRACT: Aluminum (III) and magnesium (II) interactions with the aromatic containing aminoacid side chains are studied using the B3LYP density functional. Bader and the NBO analyses have been performed on the optimized structures in order to shed light on the effect of the metal on the aromatic rings. We began by studying the interactions between the metal cations and benzene. Then a methyl was added to represent more accurately the phenylalanine functional group. We have also studied, in a similar way, the functional groups of the tyrosine and tryptophan aminoacids. The strongest bond is 447 kcal/mol, which occurs between the Al(III) and the indole. For magnesium, the strongest bond is 151 kcal/mol for the methyl–indole complex. As in the complexes of previous sections, the addition of the methyl leads to stronger binding complex, and this effect is significantly larger for aluminum than for magnesium. The NBO and Bader analyses revealed that the aromaticity of the carbon rings remains after interaction with magnesium. However, when the ring interacts with aluminum, aromaticity is lost, even though certain delocalization is kept.
Int J Quantum Chem 00: 1–23, 2002

Correspondence to: Jesus M. Ugalde; e-mail: ugalde@sq.ehu.es.
Contract grant sponsor: Basque Government (Eusko Jaurlaritza).
Contract grant sponsor: Spanish DGICYT.
Contract grant sponsor: Provincial Government of Gipuzkoa (Gipuzkoako Foru Aldundia).

Introduction

The aluminum (III) cation has gained interest throughout the chemical and biochemical world [1] after numerous negative aspects of it were reported [2–10]. Its toxicity is thought to be produced due to competition with other metal cations in biological systems. Magnesium (II) seems to be the most affected cation, since both have similar size, which is a dominant factor over the charge identity in terms of metal ion competition [4, 11]. Aluminum (III) cation binds the active site, which in a healthy system was assisted by other metal cations having specific binding and charge properties [12], disrupting the proper function of the system.

Some of these recent studies focused on the paths that this cation may take to get into the cell [13, 14], and then deposit in different parts of the organism [9, 15]. Others studied the specific interactions of aluminum (III) cation with specific chemicals [16].

Recent advances in experimental methods like electrospray ionization, charge stripping spectroscopy, double-charge spectroscopy, etc., have provided accessibility to multiple charged cations [17–19], and in particular to triply charged cations. Thus, this makes the present study very timely to rationalize the mechanism of interactions of aluminum (III) with biologically relevant systems. Naturally, an obvious extension of these studies is to account for the long range effects arising from the large domain of proteins and to include properly include the solvent, recalculate the interaction, and compare it with the bare system to extract information on the effects of the solvent. This will set the investigation of the solvation on firm grounds. As wisely indicated by Schröder and Schwarz in a recent feature article in the *Journal of Physical Chemistry*: "Nevertheless, some implications derived from fundamental studies of small, multiply charged ions... are of crucial importance for the understanding of the behavior of large molecules" [17].

Ab initio studies on metal cations and aminoacids are not abundant in the literature; especially lacking are reports including aluminum (III) interactions. However, there are some studies concerning dications and the side chain of aminoacid interactions [20–23]. Yañez's group has also studied the reactions between some monocations and formamide [24–26].

In previous works, we have studied, in the gas phase, the aluminum (III) interactions with the side chains of the acid aminoacids [27], acid derivative aminoacids [28], and sulfur-containing aminoacids [29], and we have compared our results with the magnesium (II) interactions with the same species. Overall, we observed that the binding energies for aluminum (III) were significantly larger than for magnesium (II), and that the strongest bindings occurred with the side chains of the *Asp* and *Glu* aminoacids, with values around 10 kcal/mol larger than the binding between these cations and the dehydrogenated cysteine. One important difference between both cations was found for the acidic and sulfur containing aminoacid side chains–metal complexes. According to our analysis, while the aluminum forms Lewis-type bonds to the ligand, the magnesium is only weakly bound through tiny charge transfer interactions. Similarly, for the acid derivative aminoacid side chains we found covalent bonds for the aluminum complexes while magnesium bonds were ionic. However, both the sulfur–aluminum (III) and –magnesium (II) bindings were reported to be covalent after inspection of the energy density of their bond critical points. The NBO analysis also reported bonding interactions, and not only second-order interactions, between the sulfur and the magnesium.

In the present study we focus on the aminoacid side chains containing aromatic groups: phenylalanine (*Phe*), Tyrosine (*Tyr*), and tryptophan (*Trp*). The interactions of these aromatic chains with cations, i.e., cation–π interactions, are strong noncovalent binding forces very important in many different systems (small organic molecules, supramolecules, and biochemical processes [30–36]). These interactions are dominated by electrostatic and cation-induced polarization. Recently, Cubero et al. [37] showed that these two terms drove 99% of the binding energies for various sodium (I)–π complexes. Several studies have also been carried out involving the recognition problem between metals and different aromatic compounds [38–41]. The role of ligands with aromatic moieties as to the binding to the human inmunodeficency virus type 1 integrase (HIV-1 IN) has also been recently considered [42].

Most of these studies, either experimental or theoretical, concern the monocation–π interactions, and few of them study dication–π interactions [42, 43]. In this study, we analyze the interactions between a trication [aluminum (III)] and a dication [magnesium (II)] with various aromatic moieties which resemble the aromatic aminoacid

residues. In particular, we have used benzene and toluene to represent the *Phe* side chain, and phenol and 4-methylbenzenol for *Tyr*, and indole for *Trp*, respectively. These π systems offer strong enough binding sites that can compete with more common coordinating groups, e.g., amines, alcohols, etc. Improving the understanding of these cation–π interactions should help us to learn more concerning the interactions between cations and the side chains of aromatic aminoacids.

Methods

All the geometry optimizations and frequency calculations were carried out with the GAUSSIAN 98 [44] package using the hybrid B3LYP [45, 46] approximate gradient-corrected density-functional method. The standard all-electron 6-31+G(*d*,*p*) basis set was used for the metal cations, while the relativistic compact effective core potentials and shared-exponent basis set of Stevens, Krauss, Barsch, and Jasien (SBKJ) [47] including a polarization and a diffuse function was used for atoms of the ligands. Gresh and collaborators [20–22] found that this pseudopotential/all-electron basis set combination for the ligand and the metal cation, respectively, yields reliable results.

The corresponding zero-point vibrational energy (ZPVE) corrections were made to the total energy, and the binding energy was evaluated with the ZPVE corrected energies as

$$(E_B) = E_{xl} - (E_l + E_x) \quad (1)$$

where xl stands for the complex, x for the metal, and l for the ligand.

The natural bond orbital [48] analysis and the Bader [49] analysis were used to rationalize the character of the corresponding cation–ligand interactions. Natural bond orbital analysis was performed on the polyatomic wavefunction [50] using the NBO program [48, 51] as implemented in the GAUSSIAN package and the natural atomic charges were also evaluated. The AIMPAC [52] package was employed for the Bader analysis. These calculations were performed using a standard all-electron 6-31++G(*d*,*p*) basis set on the previously optimized structures.

The MOLDEN [53] program was used to draw the figures.

Results and Discussion

As in the previous chapters, we begin by studying the interactions between the smallest representation of the aminoacid side chain (i.e., benzene and phenol for *Phe* and *Tyr*, respectively) and the cation, then adding a methyl group to represent the side chain of the aminoacid more accurately.

Various stationary points have been found on the potential energy surfaces, but our discussion will focus on the corresponding minima.

[Al(III),Mg(II)]–PHENYLALANINE AMINOACID SIDE CHAIN INTERACTIONS

The smallest representation of the functional group of *Phe* is benzene. Therefore, we start our study analyzing the interactions between both Al(III) and Mg(II) cations with benzene. Later we will add one CH_3 group to represent more accurately the aminoacid side chain. At the B3LYP/DZ(*p*,*d*) level of theory benzene has a D_{6h} symmetry, with C–C bond lengths of 1.416 Å and C–H bond lengths of 1.092 Å (see Table I).

C_{6v} symmetry pyramidal [Al(III),Mg(II)]–benzene metal on-top complexes have been found (see Fig. 1).

Upon interaction with the aluminum (III) cation, the benzene C–C bonds lengthen from 1.416 to 1.460 Å. C–H bond lengths also increase from 1.092 to 1.101 Å. The Al–C distances are 2.201 Å, slightly shorter than the Al–S distances in the $Al–SCH_3^{2+}$, and larger than the complexes of aluminum (III) with the acid and acid derivative aminoacid side chains (see previous chapters). The magnesium cation, however, does not enlarge as much the benzene ring, the C–C and C–H bonds are 1.433 and 1.093 Å, respectively, and the C–Mg distance is also larger, 2.40 Å, with a distance to the center of the ring of 1.925 Å, substantially larger than the Al–C bonds, all these values indicating weaker Mg(II)–benzene interactions.

Charge transfer interactions are observed, being significantly larger in the aluminum case. Thus, aluminum gains negative charge resulting in a total natural atomic charge of 2.134 e^-. This charge comes from the hydrogens, which loose 0.15 e^- each in the aluminum complex and 0.09 e^- each in the magnesium complex (see Table II).

The natural bond analysis shows several differences between these complexes. The NBO draws

TABLE I

Geometrical features of the benzene and toluene and their complexes. Bond lengths are given in angstroms, and dihedrals and angles are given in degrees.

	Benzene			Toluene		
	—	Al	Mg	—	Al	Mg
C1–C2	1.416	1.460	1.433	1.417	1.483	1.442
C2–C3	1.416	1.460	1.433	1.415	1.461	1.432
C3–C4	1.416	1.460	1.433	1.413	1.449	1.432
C4–C5	1.416	1.460	1.433	1.416	1.449	1.432
C1–C7	—	—	—	1.525	1.485	1.523
X–C1	—	2.201	2.400	—	2.306	2.446
X–C2	—	2.201	2.400	—	2.168	2.381
X–C3	—	2.201	2.400	—	2.205	2.371
X–C4	—	2.201	2.400	—	2.242	2.374
dh(C1C2C5C6)	—	—	—	0.0	0.0	0.0
dh(C1C2C3C5)	—	—	—	0.0	7.31	2.1
dh(C4C3C2C6)	—	—	—	0.0	0.39	0.03

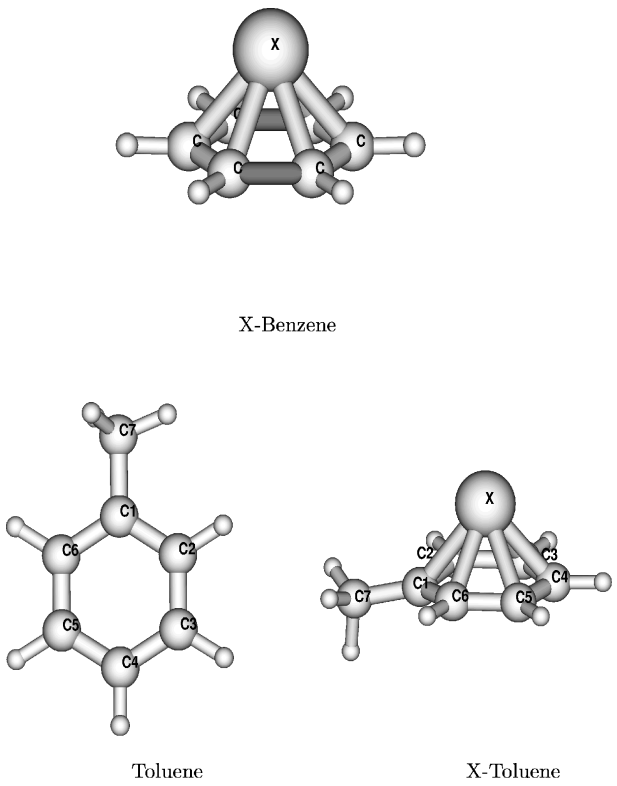

FIGURE 1. X–Benzene is the C_{6v} symmetry complex after the metal cation, X = Al(III), Mg(II), binds to benzene. Toluene, and X–toluene, the minimum corresponding to the X–toluene complexes, which has C_s symmetry.

a classical picture of the isolated benzene, i.e., a six membered ring with three alternate π bonds. The Mg(II)–benzene complex maintains the same representation for the benzene moiety. Thus, magnesium interacts with the ring by second order interactions, where the π bonds donate charge density to the empty 3*s*-orbital of Mg(II). These donations have an energetical contribution of 15.37 kcal/mol. The Al–benzene complex is described in an entirely different way. The C–C π bonds of the benzene ring disappear due to the presence of the aluminum cation. Each of the resulting singly occupied carbon *p*-orbitals interacts with two of the three empty 3*p*-orbitals of aluminum (the ones parallel to the aromatic ring plane) and contributes energetically with 15 kcal/mol each. Each σ_{C-C} bond also interacts with the Al(III) empty 3*s*-orbital, and the remaining 3*p*-orbital with energy contributions of 4.79 and 3.46 kcal/mol, respectively. Finally, the charge transfer from the Al 2*s*-orbital to each of the singly occupied carbon *p*-orbitals amounts a total contribution of 12 kcal/mol.

Concomitantly, the Bader analysis reveals that once the benzene interacts with the metal cation, the C–C bonds are activated (their energy density becomes substantially less negative). Consequently, the C–C bond distances elongate. This effect is larger for aluminum complexes, as clearly seen in Tables I and III. The electron density at the C–C bond critical points decreases, as expected, upon interaction with the metal cation, from 0.301

TABLE II
NBO charges of benzene and toluene and their complexes.

	Benzene			Toluene		
	—	Al	Mg	—	Al	Mg
X		2.134	1.822	—	2.068	1.819
C1	−0.234	−0.250	−0.299	−0.040	0.066	−0.051
C2	−0.234	−0.250	−0.299	−0.239	−0.324	−0.323
C3	−0.234	−0.250	−0.299	−0.231	−0.235	−0.294
C4	−0.234	−0.250	−0.299	−0.249	−0.283	−0.322
C5	−0.234	−0.250	−0.299	−0.232	−0.235	−0.294
C6	−0.234	−0.250	−0.299	−0.237	−0.324	−0.323
H1/C7	0.234	0.394	0.329	−0.672	−0.726	−0.706
H2	0.234	0.394	0.329	0.236	0.382	0.322
H3	0.234	0.394	0.329	0.239	0.386	0.326
H4	0.234	0.394	0.329	0.240	0.386	0.327
H5	0.234	0.394	0.329	0.239	0.386	0.326
H6	0.234	0.394	0.329	0.236	0.382	0.322

to 0.280 and 0.292 a.u., for aluminum (III) and magnesium (II), respectively. For both aluminum (III) and magnesium (II) complexes, the same critical points are located within the benzene moiety. Six X–C bond critical points, six ring critical points (located in the center of the triangles formed by two X–C and one C–C bonds), and a cage critical point along the line connecting the cation and the center of the ring have been located. All the C–C bond critical points and the ring critical point of the benzene ring have been also located.

However, metal–carbon bond properties are different for each of the cations. While the Al–C bonds are found to be covalent, i.e., the energy density at the bond critical point is negative, the Mg–C is ionic according to the topological analysis of the electron density. Notice, however, that the energy density of the Mg–C bond critical point is very small, 0.001 a.u. Cubero et al. [43] studied the topology of the electron density in various cation–π complexes, at the HF/6-31G(*d*,*p*) level of theory. They found the same topological structure of the electron density for the Mg(II)–benzene complex. The reported energy density and the laplacian at the Mg–C bond critical points are 0.024 and 0.107 a.u., while our values, despite the different level of theory, are 0.027 and 0.108 a.u.

Bader et al. [33] showed that the total charge density at the bond critical point is a characteristic for a bond of a given formal order. In Figure 2 we have plotted the charge density at the bond critical point vs. the bond length of the different C–C bonds before and after binding to the cation, together with the values of some selected simple hydrocarbons taken from Ref. [33] as a reference. These hydrocarbons are molecules with well defined bond orders of 1, 1.5, and 2. Benzene, toluene, phenol, and 1,4-methylbenzenol lie in the zone corresponding to bonds with bond order 1.5 (the small difference is due to the different levels of theory). When these ligands interact with the aluminum (III) cation, it is observed that the bonds are displaced toward the zone corresponding to bond order one. Thus, the aluminum alters significantly the aromatic character of the ligands. Similarly, the C–C bond orders of the magnesium complexes are plotted in Figure 3. It is clearly observed that the benzene ring still retains its aromatic character after binding to the magnesium cation, for its C–C bond orders remain close to 1.5.

Two stationary points within 0.5 kcal/mol were located for toluene, which is the functional group of *Phe*, at the level of theory described above. A minimum with C_s symmetry and a transition state with C_1 symmetry which has one imaginary frequency of 45.44*i* cm^{-1} corresponding to the rotation of the methyl group (the minimum is shown in Fig. 1). The aromatic carbon–methyl bond length is 1.525 Å.

Two nearly energy degenerate stationary points have also been found for the [Al(III), Mg(II)]–toluene complexes: a minimum with C_s symmetry and a C_1 transition state whose imaginary frequency corresponds to the methyl rotation. The Al–C dis-

TABLE III

Bader analysis for the benzene and toluene complexes. Charge densities (ρ), laplacian of the densities ($\nabla^2\rho$), and energy densities [$H(r)$], of the corresponding bond critical points. The ellipticities (ϵ) the X–C bonds are also given.

		Benzene			Toluene		
	X	—	Al	Mg	—	Al	Mg
C1–C2	ρ	0.301	0.280	0.292	0.300	0.270	0.289
	$\nabla^2\rho$	−0.789	−0.691	−0.746	−0.781	−0.652	−0.725
	$G(r)$	0.092	0.080	0.088	0.093	0.073	0.086
	$H(r)$	−0.289	−0.252	−0.274	−0.288	−0.236	−0.267
C2–C3	ρ	0.301	0.280	0.292	0.301	0.277	0.292
	$\nabla^2\rho$	−0.789	−0.691	−0.746	−0.789	−0.674	−0.740
	$G(r)$	0.092	0.080	0.088	0.092	0.080	0.089
	$H(r)$	−0.289	−0.252	−0.274	−0.290	−0.249	−0.274
C3–C4	ρ	0.301	0.280	0.292	0.302	0.285	0.292
	$\nabla^2\rho$	−0.789	−0.691	−0.746	−0.793	−0.714	−0.747
	$G(r)$	0.092	0.080	0.088	0.093	0.084	0.089
	$H(r)$	−0.289	−0.252	−0.274	−0.292	−0.262	−0.275
C4–C5	ρ	0.301	0.280	0.292	0.301	0.285	0.292
	$\nabla^2\rho$	−0.789	−0.691	−0.746	−0.788	−0.714	−0.747
	$G(r)$	0.092	0.080	0.088	0.092	0.084	0.089
	$H(r)$	−0.289	−0.252	−0.274	−0.289	−0.262	−0.275
C5–C6	ρ	0.301	0.28	0.292	0.302	0.277	0.292
	$\nabla^2\rho$	−0.789	−0.691	−0.746	−0.794	−0.674	−0.74
	$G(r)$	0.092	0.080	0.088	0.094	0.080	0.089
	$H(r)$	−0.289	−0.252	−0.274	−0.292	−0.249	−0.274
C6–C1	ρ	0.301	0.280	0.292	0.299	0.270	0.289
	$\nabla^2\rho$	−0.789	−0.691	−0.746	−0.776	−0.652	−0.725
	$G(r)$	0.092	0.080	0.088	0.092	0.073	0.086
	$H(r)$	−0.289	−0.252	−0.274	−0.286	−0.236	−0.267
C1–C7	ρ	—	—	—	0.246	0.258	0.244
	$\nabla^2\rho$	—	—	—	−0.569	−0.636	−0.568
	$G(r)$	—	—	—	0.055	0.085	0.064
	$H(r)$	—	—	—	−0.197	−0.244	−0.205
X–C1	ρ	—	0.051	0.027	—	—	—
	$\nabla^2\rho$	—	0.099	0.108	—	—	—
	$G(r)$	—	0.041	0.026	—	—	—
	$H(r)$	—	−0.016	0.001	—	—	—
	ϵ	—	7.535	9.583	—	—	—
X–C2	ρ	—	0.051	0.027	—	0.054	0.027
	$\nabla^2\rho$	—	0.099	0.108	—	0.107	0.115
	$G(r)$	—	0.041	0.026	—	0.045	0.028
	$H(r)$	—	−0.016	0.001	—	−0.018	0.001
	ϵ	—	7.535	9.583	—	1.721	14.16

(Continued)

TABLE III
(Continued)

		Benzene			Toluene		
	X	—	Al	Mg	—	Al	Mg
X–C3	ρ	—	0.051	0.027	—	—	0.028
	$\nabla^2\rho$	—	0.099	0.108	—	—	0.118
	$G(r)$	—	0.041	0.026	—	—	0.028
	$H(r)$	—	−0.016	0.001	—	—	0.001
	ϵ	—	7.535	9.583	—	—	11.16
X–C4	ρ	—	0.051	0.027	—	0.048	0.028
	$\nabla^2\rho$	—	0.099	0.108	—	0.099	0.118
	$G(r)$	—	0.041	0.026	—	0.04	0.028
	$H(r)$	—	−0.016	0.001	—	−0.015	0.001
	ϵ	—	7.535	9.583	—	31.31	7.970
X–C5	ρ	—	0.051	0.027	—	—	0.028
	$\nabla^2\rho$	—	0.099	0.108	—	—	0.118
	$G(r)$	—	0.041	0.026	—	—	0.028
	$H(r)$	—	−0.016	0.001	—	—	0.001
	ϵ	—	7.535	9.583	—	—	11.16
X–C6	ρ	—	0.051	0.027	—	0.054	0.027
	$\nabla^2\rho$	—	0.099	0.108	—	0.107	0.115
	$G(r)$	—	0.041	0.026	—	0.045	0.028
	$H(r)$	—	−0.016	0.001	—	−0.018	0.001
	ϵ	—	7.535	9.583	—	1.721	14.16

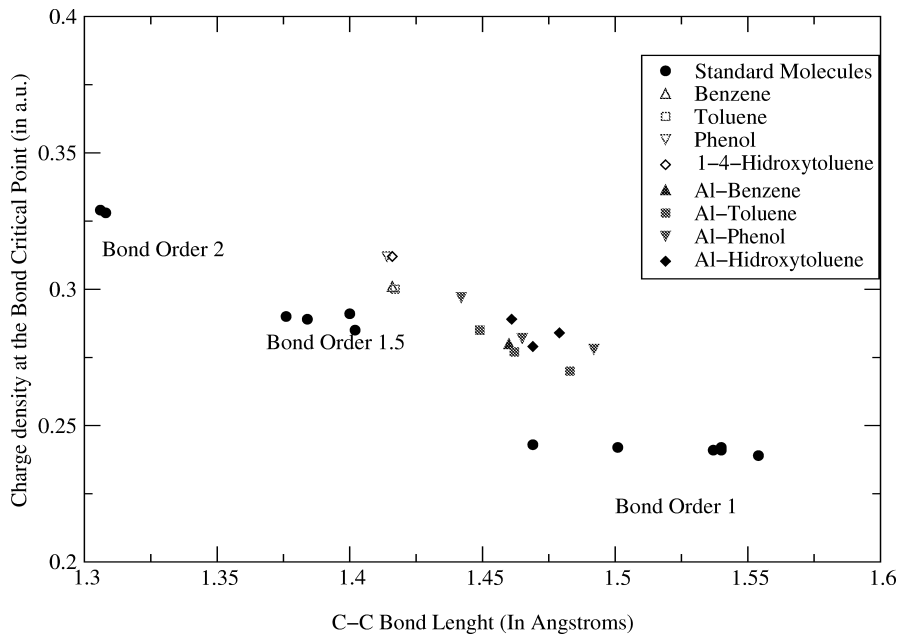

FIGURE 2. Charge densities at the bond critical points are plotted vs. the C–C bond length of the ligand before (the unfilled symbols) and after binding to the aluminum (the filled symbols). These values are compared with some hydrocarbons possessing (according to the Lewis model) known bond orders of 2 (C_2H_4N, C_3H_6O), 1.5 ($C_3H_3^+$, $C_2H_5^+$, . . .), and 1 (C_2H_6, C_4H_6, etc.). Taken from Ref. [33]. These hydrocarbons are represented by filled dots.

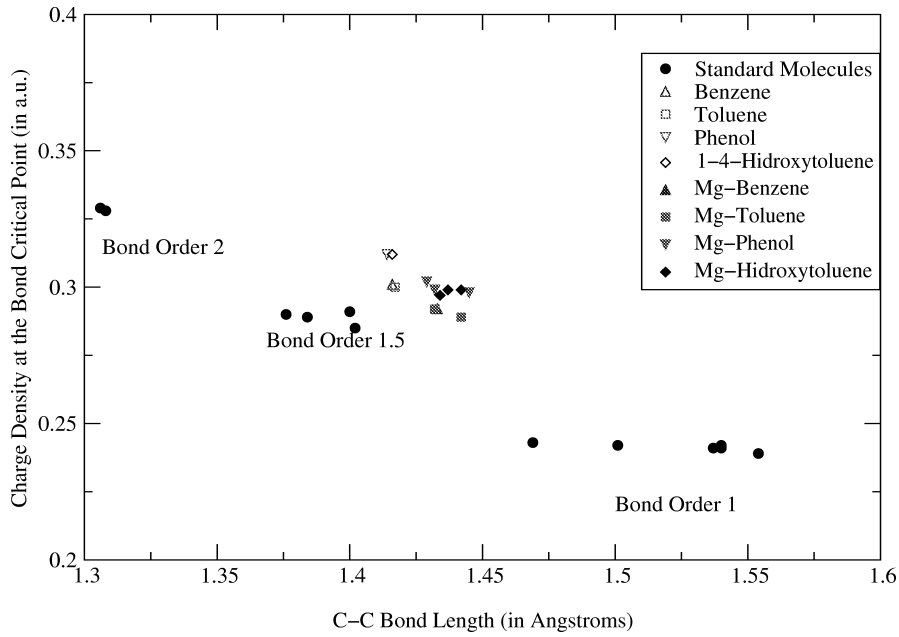

FIGURE 3. Here we show the same as in Figure 3 but for the magnesium cation.

tances span from 2.168 to 2.306 Å. The shortest bond is between the Al and C2 and C6, and the largest between aluminum and C1 (see Table I and Fig. 1 for further details). The C–C distances change slightly as compared to those in toluene, and the C–C bond between the ring and the methyl shrinks considerably from 1.525 in toluene to 1.486 Å in the aluminum complex. The ring also looses planarity; the C2, C3, C4, C5, and C6 remain in a plane, while C1 is 7° below this plane (where the aluminum cation is above the C2–C3–C4 plane).

The Mg(II)–toluene complex has Mg–C distances around 2.4 Å. As in the aluminum complex, the largest Mg–C distance occurs with C1 (2.446 Å) but the shortest bonds are with C3 and C5 (2.371 Å). The C–C bonds of the ring are 1.432 Å, except the C1–C2 and C1–C6 bonds which are slightly larger 1.442 Å. The planarity of the ring is also lost, but this effect is not as large as in the aluminum complex. The C1 carbon is the single atom lying out of the C2–C3–C5 plane by 2.10° (see Table I for further details). The C–C bond between the ring and the methyl has a length of 1.523 Å, which is almost the same as it was in toluene.

The charge transfer pattern within these complexes is similar to benzene complexes (see Table II).

The NBO description for the Al(III)–toluene complex does not report π-bonds on the aromatic ring. Thus, each of the singly occupied carbon *p*-orbitals, except C1 (which binds to the methyl group), donates some charge density to two of the aluminum *p*-orbitals with energetical contributions of around 21 kcal/mol for each. Similarly, each of the σ_{C-C} bonds donates some charge density to the aluminum with a total energy contribution of around 76 kcal/mol.

For magnesium (II), again three π_{C-C} bonds are found in the aromatic ring and these π-bonds are the ones that donate most charge density to the magnesium empty 3*s*-orbital, associated with a second order energy of 15 kcal/mol each.

The effect of the addition of the methyl group to the aromatic ligand triggers remarkable differences in the topological properties of the electron density as can be observed in Table III. A similar description to Al(III)–benzene is obtained for the C–C bonds of toluene.

However, the description of the [Al(III), Mg(II)]–C bonds differs substantially. For the Al(III)–toluene complex, bond critical points are located only for Al–C2, Al–C4, and Al–C6, i.e., the *orto* and *para* positions of toluene, having also covalent character.

Three ring critical points were also located for C1–C2–Al–C6–C1, C2–C3–C4–Al–C2, and its symmetry related ring. However, the Mg(II)–toluene complex presents bond critical points in all but the Mg–C1 bonds, with positive values of the energy

density at the bond critical point, indicating the ionic character of this complex.

A ring critical point was also located in the C1–C2–Mg–C6–C1 ring, and a cage critical point too. The bond order vs. bond length of these complexes is also plotted in Figures 2 and 3, and the same trend as in the X–benzene complexes is observed.

Another important feature reported by the Bader analysis is the high ellipticities of the X–C bond critical points as are observed in Table III. This fact, together with the small differences between the charge density of the ring and bond critical points, is indicative of strong delocalization of the electron density responsible for the binding over the conical surface defined by the metal atom and the carbon atoms of the ring [54]. The charge densities at the ring critical points are 0.050 and 0.027 for Al(III)– and Mg(II)–benzene complexes respectively, and 0.047 and 0.025 for Al(III)– and Mg(II)–toluene complexes, respectively (note that we leave aside the ring critical point corresponding to the ring formed between C1–C2–X–C6–C1 where the densities are smaller). The ellipticities of the *orto* Al–C bonds of the Al(III)–toluene complex decrease substantially, whereas the ellipticity of the *para* bond increases dramatically. The λ_2 of these critical points and the adjacent ring critical points are very small, −0.001 and 0.002, respectively. Thus, the Al–C4 bond may easily collapse into a different binding scheme nearly degenerate in energy, the only possibilities being either the formation of the Al–C3 bond or Al–C5 bond.

This description agrees with the NBO picture. Both methods reveal a certain delocalization in benzene when it interacts with the metal cations. In the aluminum (III) cation, however, the aromaticity of the ring is lost, and this delocalization is due to the equivalent singly occupied *p*-orbitals, which interact with the aluminum cation instead of with themselves to build the aromatic structure of the ring π-bonds between the carbons. The Mg(II)–benzene complex has the π-bonds of the ring and therefore retains the aromaticity of the ring.

The binding energies between the benzene and Al(III) and Mg(II) cations are 368.7 and 125.1 kcal/mol, respectively (see Table IV). These energies are slightly larger for toluene, 404.5 kcal/mol for aluminum, and 133.4 for magnesium. Cubero et al. [43] reported a binding energy of 118 kcal/mol for the Mg(II)–benzene complex at the HF/6-31G(*d*,*p*) level of theory. Nicklaus et al. [42] gave the HF/6-311G** binding energy of 114.6 kcal/mol. These binding energies are very similar to the binding between these cations and the acid derivative aminoacid side chains (approximately 400 for aluminum and 145 kcal/mol for magnesium), and larger than the binding with the neutral cysteine and methionine sulfur containing aminoacid side chains. However, the negatively charged aminoacid side chains bind significantly stronger to aluminum and magnesium. Their binding energies are approximately 740 and 360 kcal/mol, respectively.

[Al(III), Mg(II)]–TYROSINE AMINOACID CHAIN INTERACTIONS

The tyrosine aminoacid has a phenol as the simplest representation of the functional group of its side chain. Two phenol isomers have been located at the B3LYP/DZ(*d*,*p*) level of theory.

A planar minimum and a transition state 2.8 kcal/mol higher in energy, with the OH dihedral angle close to 90° with respect to the ring, are present. The imaginary frequency ($324i\ \mathrm{cm}^{-1}$) of this transition state corresponds to the rotation of the hydroxyl group. The C–C bond lengths of the ring are near 1.41 Å, and the C–O bond is 1.383 Å (see Table V for more details).

Three different stationary points were located for the Al(III)–phenol complex. A minimum (see Fig. 4), where the phenol's hydroxyl group is perpendicular to the Al–C orientation, and two transitions states, which arise after the rotation of the hydroxyl group, 7 and 12 kcal/mol higher in energy.

After interacting with the aluminum, the phenol planarity is lost, the carbon bound to the hydroxyl, C1, is 14° out of the plane formed by the rest of the carbon atoms. The C–C distances in the ring also change slightly (see Table V), while the largest change occurs at the C–C bonds involving C1, which elongates 0.08 Å. The Al–C distances are approximately 2.2 Å for the bonds between Al and carbon atoms situated on the plane, while the Al–C1 bond length is significantly larger, 2.398 Å.

For magnesium, the analogous structures of the Al(III)–phenol minimum and the transition states were also found, with energy differences of 5 and 9 kcal/mol with respect to the minimum. Magnesium also breaks the planarity of the phenol ring, but the deformation induced in the ring is not as large as in the Al(III)–phenol complex. The C1 atom is only 6° out of the C2–C3–C4 plane. The Mg–C distances are also larger than the corresponding Al–C ones, being close to 2.4 Å (see Table V for details), and again the Mg–C1 is slightly larger than the oth-

TABLE IV

ZPVE corrected total energies (in hartrees) and binding energies of the studied complexes (in kcal/mol). S stands for the corresponding isomer.

		E	BE	S
Benzene	—	−37.405289	—	
	Al	−278.39504	−378.70	
	Mg	−236.831324	−125.09	
Toluene	—	−44.240656	—	
	Al	−285.271573	−404.53	
	Mg	−243.67997	−133.43	
Phenol	—	−53.380287		
	Al	−294.40239	−399.00	
	Mg	−252.81257	−129.02	Pyr
	Mg	−252.806698	−125.33	Mono
Methylbenzenol	—	−60.214726	—	
	Al	−301.267798	−418.43	
	Mg	−259.658629	−136.31	Pyr
	Mg	−259.650868	−131.44	Mono
Indole	—	−59.185339	—	
	Al	−300.286572	−447.94	X–c3
	Mg	−258.633253	−138.35	X–c3
	Mg	−258.647079	−147.02	X–Pyr
	Mg	−258.616107	−127.59	X–c2
	Mg	−258.614495	−126.58	X–c9
Methyl–indole	—	−66.020364	—	
	Al	—	—	—
	Mg	−265.474415	−142.20	X–c3
	Mg	−265.489432	−151.62	X–Pyr
	Mg	−265.465579	−136.66	X–c2
	Mg	−265.459622	−132.92	X–c9

ers with a bond length of 2.517 Å. The C–C distances change slightly with respect to phenol, this change being smaller than that caused by the aluminum.

The charge transferred from the ring to the metal cation is very similar to the ones observed for toluene complexes as observed in Table VI.

The NBO descriptions of these complexes are similar to the X–benzene ones. While the aluminum promotes breaking of the aromatic π_{C-C} bonds, magnesium does not. The singly occupied carbon *p*-orbitals (except C1 is which is bound to the oxygen) interact with the aluminum *p*-orbitals with an overall energy contribution of 105 kcal/mol. There are also donations from each σ_{C-C} to the aluminum *s*- and *p*-orbitals. In this case each σ_{C-C} bond contributes ∼11 kcal/mol. The magnesium complex is described as the Mg(II)–benzene complex. In this case the π_{C-C} interactions with the magnesium are around 15 kcal/mol, an order of magnitude less as compared with the Al(III)–phenol complex.

At first glance, the electron density topological analysis of these complexes gives a different description compared to the NBO analysis. NBO reports similar interactions between all the carbons and the metal cation. The Bader analysis, however, discriminates between the different carbon atoms and the B3LYP/6-31++G** density has bond critical points between the Al–C2 and Al–C6 (see Table VII). Similarly, magnesium also binds to some but not all the ring's atoms, namely, C2, C4, and C5. Note that as for the previous complexes the ellipticities of the X–C bonds are large, especially for magnesium, and the ring and bond critical point densities are also very similar, indicating the delocalization

TABLE V

Geometrical features (in angstroms) of phenol, methylbenzenol, and their complexes. Mg (O) stands for the Mg–oxygen binding complex. dh1 stands for the C6C2C3C5 dihedral, and dh2, dh3, dh4, and dh5 stand for the C1C2C3C5, C4C3C2C6, MGOC1C2, and H6C6C1C2 dihedrals, respectively.

	Phenol				Methylbenzenol			
X	—	Al	Mg	Mg (O)	—	Al	MG	Mg (O)
C1–O	1.380	1.281	1.328	1.440	1.385	1.289	1.333	1.442
C1–C2	1.417	1.492	1.445	1.392	1.416	1.479	1.442	1.39
C2–C3	1.414	1.465	1.432	1.429	1.412	1.469	1.434	1.425
C3–C4	1.414	1.442	1.429	1.423	1.418	1.461	1.437	1.432
C4–C5	1.416	1.448	1.434	1.406	1.417	1.468	1.442	1.413
C5–C6	1.412	1.460	1.427	1.443	1.412	1.461	1.428	1.441
C6–C1	1.416	1.492	1.446	1.445	1.413	1.481	1.443	1.442
C4–C7	—	—	—	—	1.526	1.508	1.523	1.52
X–C1	—	2.398	2.517	—	—	2.393	2.495	—
X–C2	—	2.176	2.406	—	—	2.166	2.382	—
X–C3	—	2.224	2.379	—	—	2.174	2.356	—
X–C4	—	2.260	2.364	—	—	2.299	2.398	—
X–C5	—	2.216	2.365	—	—	2.174	2.347	—
X–C6	—	2.178	2.397	—	—	2.176	2.378	—
X–O	—	—	—	2.012	—	—	—	2.007
dh1	0	0.4	0.3	1.1	0.0	0.4	0.2	1.2
dh2	0	14.1	5.8	1.5	0.0	11.5	5.5	1.7
dh3	0	0.4	0.7	2.9	0	5.0	1.1	2.9
dh4				133.9				132.6
dh5				146.0				147.5

of the charge density. HF and MP2 geometry optimizations with the basis set described above were also carried out for these complexes and the Bader analysis was carried out for the HF and MP2 densities (note that the geometries are very similar and we omit them for the sake of brevity). These densities gave a different binding scheme as compared with the B3LYP density, which should not be surprising due the properties of these charge densities. For Al(III)–phenol both densities have Al–C bonds in the *orto* and *para* positions of the aromatic ring.

The *para* position has a high ellipticity, 30 and 3 at the MP2 and HF densities, respectively. Here, the same reasoning as in the Al(III)–toluene complex case may be applied. Note also that the point corresponding to the Al(III)–phenol complex in Figure 2, which lies nearest to bond order 1.5, represents the charge density at the bond critical point of the C3–C4 and C4–C5 bonds. For the Mg(II)–toluene complex the three different densities gave different binding schemes: MP2 reports bonds between Mg–C4 ($\epsilon = 6.2$) and Mg–C5 ($\epsilon = 9.1$), and HF gives Mg–C2 ($\epsilon = 5.6$), Mg–C4 ($\epsilon = 3.8$), Mg–C5 ($\epsilon = 26.7$), and Mg–C6 ($\epsilon = 99.47$), where, for all the remaining densities, the ring critical points have nearly the same charge density as the bond critical points. This confirms the higher delocalization of the charge density in the magnesium complex where the density seems to be delocalized all over the ring surface, while for aluminum there is delocalization over the C3, C4, and C5 atoms. Finally, notice that a small change in the charge density due to the differences between the levels of theory used yields different bonding schemes. This further confirms the delocalization of the charge density over the ring.

Even though discrepancies are found between the different levels of theory for the critical points involving the cation and aromatic carbons, there are some common characteristics: (i) The cage and ring critical points of the carbon rings are the same. (ii) All the Al–C bonds have covalent character while the Mg–C bonds are given to be ionic

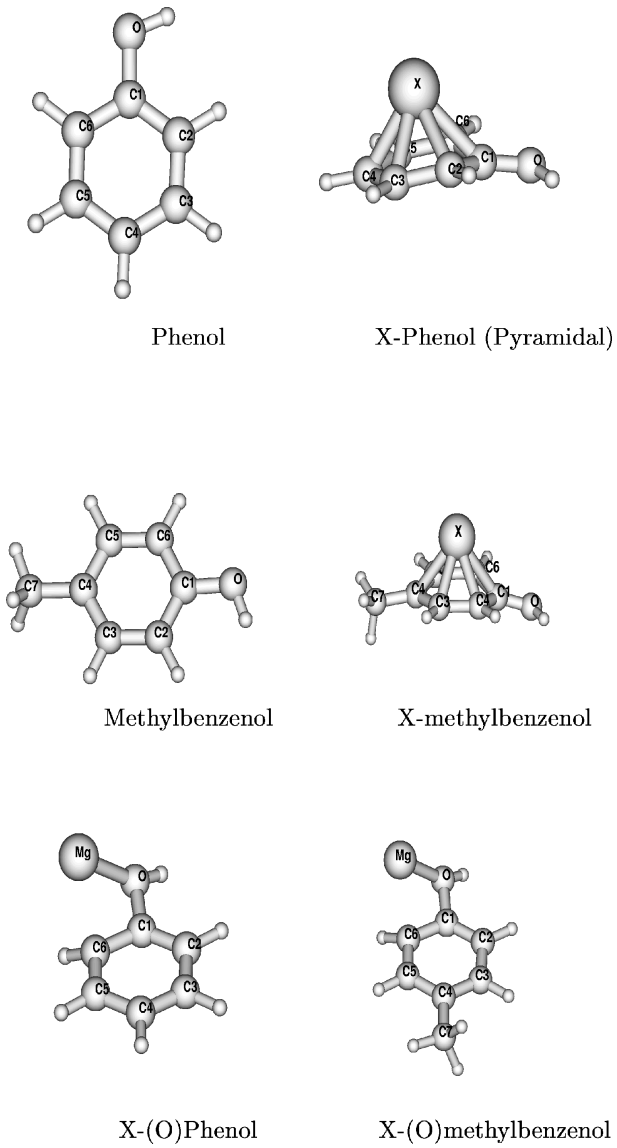

FIGURE 4. The phenol and the 1-4-methylbenzenol are shown in this figure, and the corresponding metal–ligand complexes, the pyramidal complexes, and the O-binding complexes.

[i.e., $H(r) < 0$ the former and $H(r) > 0$ the later]. (iii) The description of the ring is also very similar and the numbers differ slightly among the different levels of theory. In agreement with the geometrical observation of these complexes, the C–C elongation produced by the cation interactions with phenol is associated with the energy density decrease at the bond critical point. Similarly, the C–O bond length reduction agrees with the energy density increase observed at the bond critical point.

Next we added a methyl group in the *para* position of the aromatic ring to account for the functional group of *Tyr*. We found three stationary points of the 4-methylbenzenol within 2.5 kcal/mol. The minimum (see Fig. 4) has a C_s symmetry where the hydroxyl and methyl groups are in a staggered orientation. The C–C and C–O bond lengths of the hydroxyl ring are very similar to the phenol bond lengths, and the new C–C bond length between the methyl and the ring is 1.526 Å.

Three Al(III)–methylbenzenol stationary points were located, namely, a minimum (see Fig. 4), and two transition states, 8 and 11 kcal/mol higher in energy, respectively. These stationary points correspond to different conformers after rotations of the methyl and/or hydroxyl groups. These complexes also lose the planarity of the ring. Not only the carbon bound to the hydroxyl (C1) but also the one bound to the methyl (C4) moves out the plane formed by the remaining four carbon atoms, by 11.4° and 5.0°, respectively. The Al–C distances are slightly shorter than the Al(III)–phenol complex, as shown in Table V, except the Al–C4 bond, which is larger since this atom is now out of the plane. The C–C bonds in the ring elongate, changing from 1.41 Å to values around 1.46 Å, with the exception of the bonds where C1 is involved, which have bond lengths slightly larger, around 1.48 Å.

Three Mg(II)–methylbenzenol complexes were also located, a minimum (see Fig. 4), and two transition states, 4 and 9 kcal/mol higher in energy. The effect of the magnesium on the ligand is not as pronounced as that of the aluminum (III) cation. The ligand looses its planarity, but C1 is only 5.5° out of the C2–C3–C5 plane, while C4 is 1° out of plane. The increase of the C–C bond lengths of the ring is smaller than it was in the aluminum complex. The Mg–C bond lengths are near 2.35 Å, except Mg–C1 which is 2.485 Å, and are larger than the corresponding Al–C bond lengths.

The Bader analysis of these X–methylbenzenol complexes presents similar features to the former ones. The covalent and ionic bond character is conserved for aluminum and magnesium bonds, respectively. B3LYP density gives the same binding scheme as the Al(III)–phenol complex, and HF gives [as it does for the Al(III)–phenol complex] *orto* and *para* bonds where the *para* complex has the same properties as the Al(III)–phenol equivalent *para* bond. For the magnesium complex bond critical points are found for Mg–C3 and Mg–C5 bonds, again with very high ellipticities. The HF optimized density, however, again gives a different binding

TABLE VI
NBO charges of phenol, methylbenzenol, and its complexes.

	Phenol				Methylbenzenol			
X	—	Al	Mg	Mg-mono	—	Al	Mg	Mg-mono
X	—	2.025	1.802	1.778	—	2.021	1.80	1.766
C1	0.308	−0.426	0.325	0.272	0.300	0.423	0.305	0.255
C2	−0.318	0.464	−0.415	−0.266	−0.279	−0.407	−0.368	−0.263
C3	−0.220	−0.217	−0.275	−0.066	−0.216	−0.274	−0.300	−0.066
C4	−0.270	−0.316	−0.362	−0.214	−0.069	−0.037	−0.119	−0.002
C5	−0.220	−0.221	−0.281	−0.097	−0.217	−0.272	−0.297	−0.112
C6	−0.286	−0.385	−0.380	−0.648	−0.279	−0.361	−0.405	−0.627
O	−0.709	−0.485	−0.618	−0.884	−0.711	−0.512	−0.627	−0.888
Ho	0.504	0.616	0.559	0.602	0.503	0.607	0.556	0.601
H2	0.234	0.384	0.322	0.304	0.233	0.380	0.335	0.302
H3	0.241	0.387	0.327	0.302	0.237	0.379	0.322	0.295
H4/C	0.241	0.388	0.329	0.306	−0.671	−0.716	−0.701	−0.695
H5	0.241	0.389	0.328	0.297	0.237	0.380	0.321	0.291
H6	0.252	0.398	0.337	0.312	0.251	0.393	0.320	0.310

scheme; now bonds are reported for the *orto* and *para* position, and other topological features similar to the Mg complexes described above, indicating again the large delocalization of the charge density in the ring.

The NBO analysis for the aluminum complex reports two π_{C-C} bonds between C2–C3 and C5–C6. Each of these π-bonds donates electron density to the aluminum empty *p*-orbitals with an energy contribution of 174 kcal/mol each. Finally, the aluminum 3*s*-orbital, which populates due to the donations coming mainly from the C2–C3 and C5–C6 π-bonds, has an occupation of 0.6 e^-. Remarkably it donates back some electron density to the singly occupied C1 and C4 *p*-orbitals. The magnesium, as in all the previous complexes, is bound to the aromatic ligand due to the second order interactions occurring from the three π_{C-C} bonds to the magnesium 3*s*-orbital, each one having an energetic value around 15 kcal/mol, the same as in the previous magnesium (II) complexes. The C–C bond order vs. bond length for the X–phenol and X–methylbenzenol complexes is plotted in Figures 2 and 3.

Beside these complexes, a minimum where the magnesium interacts with the oxygen was also found for both phenol and 4-methylbenzenol. It lies around 5 kcal/mol higher in energy than the pyramidal complexes (see Fig. 4). The Mg–O bond lengths are 2.012 for the former and 2.007 Å for the later. The magnesium is out of the ring's plane by 57° in both cases, and the hydrogen bound to C6 is also out of the plane by 36°, due to the Mg–C6 interactions. The charge transfer in these complexes is slightly larger than the pyramidal complexes (the magnesium gains −0.22 e^-). The Bader analysis reports an ionic bond between the Mg and the oxygen but also reports a covalent bond between the Mg and C6 for the Mg(II)–phenol complex, and ionic for the Mg(II)–methylbenzenol case. The NBO analysis describes two π_{C-C} bonds between C1–C2 and C4–C5, and a Mg–C6 bond is reported but not a Mg–O bonds. Magnesium oxygen second order interactions between the oxygen lone pairs and the σ^*_{Mg-C} orbitals contribute 11 kcal/mol. These bonds are formed between a carbon *p*-orbital and the magnesium *s*-orbital. For the Mg(II)–methylbenzenol complex, the NBO analysis describes the ligand–cation binding as second order interactions. These interactions are large between the carbon and magnesium. There is an electron density donation from the singly occupied carbon *p*-orbital to the empty magnesium 3*s*-orbital of 68 kcal/mol, while both oxygen lone pairs interact with the magnesium 3*s*-orbital, having an energetical contribution around 7 kcal/mol each.

The binding energies for the Al(III)–methylbenzenol and the Mg(II)–methylbenzenol complexes are 418 and 136 kcal/mol, respectively,

TABLE VII

Bader analysis of phenol, toluene, and the corresponding complexes. Charge densities (ρ), laplacian of the densities ($\nabla^2\rho$), and energy densities [$H(r)$] of the corresponding bond critical points.

		Phenol				Methylbenzenol			
		—	Al	Mg	Mg–(O)	—	Al	Mg	Mg–(O)
C1–C2	ρ	0.302	0.267	0.288	0.312	0.303	0.275	0.291	0.32
	$\nabla^2\rho$	−0.799	−0.647	−0.732	−0.863	−0.8	−0.691	−0.758	−1.018
	$G(r)$	0.094	0.070	0.085	0.111	0.094	0.071	0.0834	0.115
	$H(r)$	−0.294	−0.232	−0.268	−0.327	−0.294	−0.244	−0.273	−0.370
C2–C3	ρ	0.300	0.274	0.290	0.294	0.301	0.275	0.292	0.306
	$\nabla^2\rho$	−0.779	−0.657	−0.729	−0.764	−0.782	−0.663	−0.737	−0.899
	$G(r)$	0.093	0.079	0.089	0.086	0.094	0.081	0.091	0.081
	$H(r)$	−0.288	−0.244	−0.271	−0.277	−0.289	−0.247	−0.275	−0.306
C3–C4	ρ	0.301	0.288	0.293	0.299	0.300	0.276	0.288	0.304
	$\nabla^2\rho$	−0.788	−0.725	−0.748	−0.794	−0.776	−0.675	−0.72	−0.896
	$G(r)$	0.093	0.086	0.090	0.088	0.093	0.078	0.086	0.081
	$H(r)$	−0.290	−0.268	−0.277	−0.286	−0.287	−0.247	−0.266	−0.305
C4–C5	ρ	0.300	0.285	0.291	0.307	0.301	0.281	0.292	0.313
	$\nabla^2\rho$	−0.784	−0.714	−0.738	−0.827	−0.776	−0.688	−0.730	−0.934
	$G(r)$	0.092	0.084	0.088	0.097	0.093	0.081	0.088	0.091
	$H(r)$	−0.288	−0.263	−0.273	−0.304	−0.287	−0.253	−0.271	−0.324
C5–C6	ρ	0.301	0.277	0.293	0.285	0.301	0.271	0.288	0.295
	$\nabla^2\rho$	−0.788	−0.974	−0.744	−0.721	−0.787	−0.639	−0.719	−0.847
	$G(r)$	0.094	0.081	0.091	0.08	0.094	0.079	0.089	0.076
	$H(r)$	−0.291	−0.324	−0.277	−0.261	−0.291	−0.239	−0.269	−0.288
C6–C1	ρ	0.304	0.270	0.290	0.288	0.305	0.273	0.29	0.297
	$\nabla^2\rho$	−0.818	−0.669	−0.752	−0.730	−0.824	−0.669	−0.738	−0.861
	$G(r)$	0.093	0.068	0.082	0.087	0.094	0.073	0.086	0.087
	$H(r)$	−0.297	−0.235	−0.270	−0.269	−0.3	−0.240	−0.271	−0.302
C1–O	ρ	0.276	0.349	0.318	0.237	0.275	0.344	0.315	0.231
	$\nabla^2\rho$	−0.413	−0.522	−0.423	−0.341	−0.414	−0.245	−0.443	−0.085
	$G(r)$	0.312	0.530	0.403	0.238	0.309	0.502	0.391	0.33
	$H(r)$	−0.415	−0.661	−0.509	−0.323	−0.412	−0.563	−0.502	−0.351
C4–C8	ρ	—	—	—	—	0.245	0.245	0.243	0.255
	$\nabla^2\rho$	—	—	—	—	−0.563	−0.577	−0.559	−0.699
	$G(r)$	—	—	—	—	0.055	0.078	0.063	0.059
	$H(r)$	—	—	—	—	−0.196	−0.222	−0.203	−0.234
X–C1	ρ	—	—	—	—	—	—	—	—
	$\nabla^2\rho$	—	—	—	—	—	—	—	—
	$G(r)$	—	—	—	—	—	—	—	—
	$H(r)$	—	—	—	—	—	—	—	—
	ϵ	—	—	—	—	—	—	—	—
X–C2	ρ	—	0.547	0.027	—	—	0.054	—	—
	$\nabla^2\rho$	—	0.098	0.109	—	—	0.109	—	—
	$G(r)$	—	0.043	0.027	—	—	0.045	—	—
	$H(r)$	—	−0.019	0.001	—	—	−0.018	—	—
	ϵ	—	1.189	11.825	—	—	3.124	—	—

(Continued)

TABLE VII
(Continued)

		Phenol				Methylbenzenol			
		—	Al	Mg	Mg–(O)	—	Al	Mg	Mg–(O)
X–C3	ρ	—	—	—	—	—	—	0.028	—
	$\nabla^2\rho$	—	—	—	—	—	—	0.121	—
	$G(r)$	—	—	—	—	—	—	0.029	—
	$H(r)$	—	—	—	—	—	—	0.001	—
	ϵ	—	—	—	—	—	—	6.964	—
X–C4	ρ	—	—	0.028	—	—	—	—	—
	$\nabla^2\rho$	—	—	0.122	—	—	—	—	—
	$G(r)$	—	—	0.029	—	—	—	—	—
	$H(r)$	—	—	0.001	—	—	—	—	—
	ϵ	—	—	4.651	—	—	—	—	—
X–C5	ρ	—	—	0.028	—	—	—	0.029	—
	$\nabla^2\rho$	—	—	0.119	—	—	—	0.123	—
	$G(r)$	—	—	0.029	—	—	—	0.030	—
	$H(r)$	—	—	0.001	—	—	—	0.001	—
	ϵ	—	—	13.133	—	—	—	5.771	—
X–C6	ρ	—	0.055	—	0.036	—	0.055	—	0.035
	$\nabla^2\rho$	—	0.094	—	0.151	—	0.116	—	0.164
	$G(r)$	—	0.043	—	0.038	—	0.047	—	0.040
	$H(r)$	—	−0.019	—	−0.001	—	−0.018	—	0.001
	ϵ	—	0.999	—	0.013	—	2.043	—	0.169
X–O	ρ	—	—	—	0.04	—	—	—	0.039
	$\nabla^2\rho$	—	—	—	0.306	—	—	—	0.329
	$G(r)$	—	—	—	0.065	—	—	—	0.069
	$H(r)$	—	—	—	0.011	—	—	—	0.013
	ϵ	—	—	—	0.023	—	—	—	0.013

∼20 kcal/mol larger than the X–phenol complexes (see Table IV).

The oxygen binding magnesium complex has a binding energy of 131 kcal/mol, only 5 kcal/mol lower than the Mg(II)–methylbenzenol. Compared with the X–toluene complexes, the aluminum complex is 14 kcal/mol stronger while Mg(II)–methylbenzenol is only 3 kcal/mol stronger.

TRYPTOPHAN AMINOACID CHAIN INTERACTIONS

Tryptophan is the third aminoacid which contains aromatic rings in its functional group. The indole, an aromatic compound formed by a benzene and pyrrole, has widely been used to represent tryptophan [38, 55]. These two rings present two binding sites for the metal cations. The resonance forms of indole concentrate negative charge on atoms C3 on one ring and C5, C6, and C8 on the other (see Fig. 5). In addition, the nitrogen may also bind to the metal cation. Thus, all these possibilities have been analyzed.

The geometrical features of the indole are shown in Table VIII. The C–C bond lengths are ∼1.4 Å. The NBO charges show the largest charge concentration on the nitrogen atom ($-0.57\ e^-$), while the carbon atoms have charges near $-0.25\ e^-$, with the exception of C2 and C3 with negative charges of -0.04 and $-0.32\ e^-$, respectively, and C9 which has a positive charge of $0.14\ e^-$. The hydrogen atoms have positive charges with values near $0.25\ e^-$, except H9 (bound to the N) which has a positive value of 0.44 (the NBO charges are tabulated in Table IX).

Among all the previously described binding possibilities between the indole and the aluminum (III)

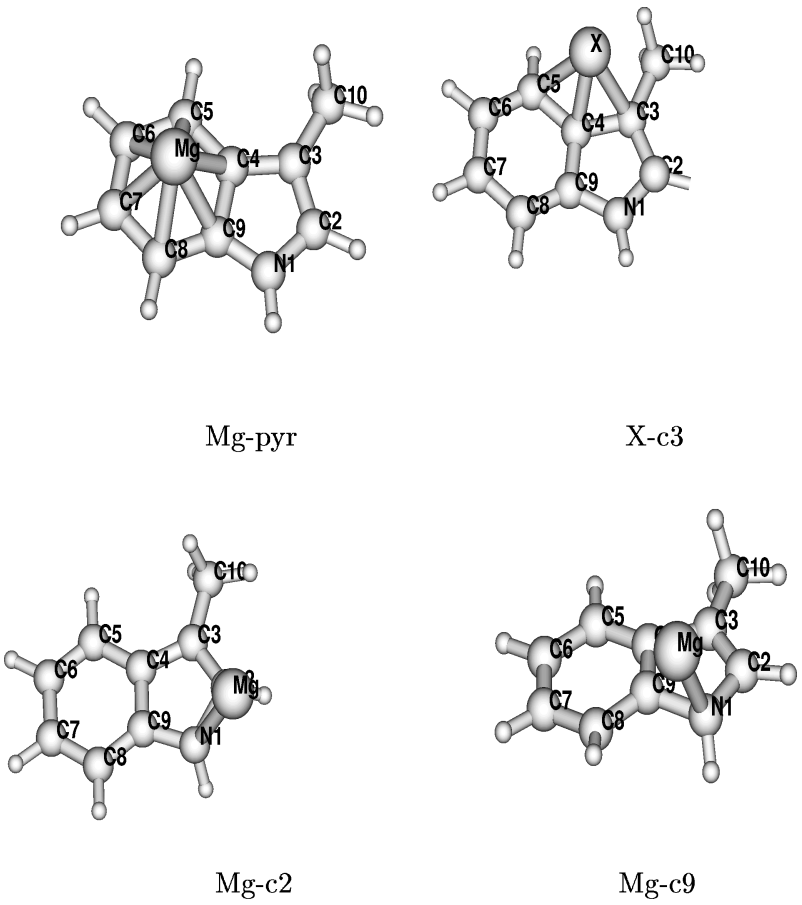

FIGURE 5. Structures corresponding to the X–methylindole complexes (note that the indole and X–indole complexes are analogous to these ones). X–Pyr is the structure where the metal cation interacts with the benzene ring of the indole. X–c3: The metal cation interacts with three carbon atoms (C3, C4, and C5) and is located outside of the rings. X–c2: The metal cation is interacting with the nitrogen and C2. X–c9: The metal cation is interacting with the nitrogen and C9.

cation, only one aluminum (III)–indole stable complex has been found (**X-c3** in Fig. 5). The indole modifies substantially its geometrical parameters upon interacting with the aluminum (see Table VIII). The biggest change is the loss of planarity; e.g., the dihedral angle for C2–C3–C4–C5 is 23°. The Al–C distances are 2.039, 2.192, and 2.080 Å with respect to C3, C4, and C5 atoms, respectively. The C–C/N bonds of the indole also change substantially. A charge density rearrangement is also observed in the indole. The aluminum withdraws electron density, resulting in a total atomic charge of 1.976 e^-. C3 and C5 are around 0.4 e^- more negative in the complex than they were in the indole, while the charge of C4 remains unaltered. With the previously mentioned exceptions, overall, the atoms of indole gain in positive charge after interacting with the aluminum.

The Bader analysis (see Table X) of this complex reveals covalent bonds between Al–C3 and Al–C5 but does not locate any critical point between Al and C4. Similarly, the NBO analysis describes Lewis bonds between the same atoms. Besides these bonds, some remarkable second other interactions are described by the NBO analysis, the strongest being charge donations going from the $\sigma_{Al–C3}$ to the antibonding $\sigma^*_{Al–C4}$ and vice versa having each an energetic contribution of 22 kcal/mol.

The $\sigma_{Al–C3}$ bond also donates electron density to the $\pi^*_{N1–C2}$ and $\pi^*_{C4–C9}$ orbitals, which contribute with 11.49 and 16.20 kcal/mol, respectively. There is a π-bond break in the indole; the NBO reports four π-bonds for the indole, but after binding to aluminum two of these bonds are broken, and the remaining singly occupied out-of-the-plane indole orbitals interact with aluminum.

TABLE VIII

Indole, methylindole, and the corresponding X–c3 complex geometrical features (in angstroms).

	Indole			Methyl–indole	
	—	Al	Mg	—	Mg
N1–C2	1.394	1.322	1.351	1.397	1.368
C2–C3	1.387	1.502	1.432	1.388	1.411
C3–C4	1.452	1.517	1.494	1.457	1.460
C4–C5	1.424	1.479	1.447	1.423	1.462
C5–C6	1.406	1.483	1.424	1.406	1.430
C6–C7	1.430	1.423	1.424	1.429	1.418
C7–C8	1.407	1.418	1.412	1.408	1.419
C8–C9	1.416	1.450	1.417	1.415	1.413
C9–N1	1.393	1.442	1.410	1.435	1.392
C9–C4	1.436	1.391	1.426	1.391	1.436
C3–C10	—	—	—	1.515	1.524
X–N1	—	—	—	—	—
X–C2	—	—	—	—	—
X–C3	—	2.039	2.23	—	2.363
X–C4	—	2.192	2.213	—	2.222
X–C5	—	2.080	2.351	—	2.238
X–C6	—	—	—	—	—
X–C7	—	—	—	—	—
X–C8	—	—	—	—	—
X–C9	—	—	—	—	—
X–C10	—	—	—	—	2.591

TABLE IX

NBO charges for indole, methylindole, and the corresponding X–c3 complexes.

	Indole			Methyl–indole	
X	—	Al (3*c*)	Mg (3*c*)	—	Mg (3*c*)
X	—	1.976	1.761	—	1.742
N1	−0.574	−0.466	−0.507	−0.580	−0.516
C2	−0.043	0.290	0.132	−0.041	0.084
C3	−0.315	−0.723	−0.658	−0.105	−0.307
C4	−0.100	−0.106	−0.178	−0.096	−0.192
C5	−0.219	−0.678	−0.500	−0.220	−0.538
C6	−0.264	0.061	−0.136	−0.262	−0.140
C7	−0.244	−0.211	−0.202	−0.245	−0.210
C8	−0.271	0.003	−0.154	−0.265	−0.131
C9	0.142	0.177	0.116	0.148	0.138
H1	0.443	0.538	0.498	0.440	0.493
H2	0.238	0.346	0.304	0.236	0.295
H3/C10	0.252	0.387	0.327	−0.670	−0.675
H5	0.240	0.388	0.303	0.239	0.305
H6	0.240	0.332	0.296	0.238	0.294
H7	0.239	0.348	0.300	0.238	0.299
H8	0.239	0.337	0.298	0.238	0.296

TABLE X

Bader analysis for indole, methylindole, and the X–c3 complex charge densities (ρ), laplacian of the densities ($\nabla^2\rho$), and energy densities [$H(r)$] of the corresponding bond critical points.

		Indole			Methyl–indole	
X		—	Al	Mg (3*c*)	—	Mg (3*c*)
N1-C2	ρ	0.296	0.346	0.325	0.293	0.3134
	$\nabla^2\rho$	−0.733	−0.720	−0.738	−0.752	−0.772
	$G(r)$	0.272	0.404	0.346	0.256	0.307
	$H(r)$	−0.455	−0.584	−0.531	−0.444	−0.500
C2–C3	ρ	0.313	0.260	0.294	0.316	0.303
	$\nabla^2\rho$	−0.825	−0.617	−0.750	−0.834	−0.776
	$G(r)$	0.112	0.064	0.090	0.115	0.100
	$H(r)$	−0.318	−0.218	−0.278	−0.323	−0.294
C3–C4	ρ	0.285	0.248	0.256	0.277	0.273
	$\nabla^2\rho$	−0.703	−0.524	−0.563	−0.663	−0.625
	$G(r)$	0.086	0.072	0.076	0.081	0.087
	$H(r)$	−0.262	−0.203	−0.216	−0.247	−0.244
C4–C5	ρ	0.283	0.265	0.280	0.295	0.272
	$\nabla^2\rho$	−0.702	−0.610	−0.680	−0.761	−0.646
	$G(r)$	0.082	0.0780	0.085	0.088	0.080
	$H(r)$	−0.257	−0.231	−0.255	−0.278	−0.242
C5–C6	ρ	0.295	0.266	0.295	0.304	0.291
	$\nabla^2\rho$	−0.742	−0.644	−0.759	−0.798	−0.744
	$G(r)$	0.092	0.0673	0.089	0.098	0.087
	$H(r)$	−0.278	−0.228	−0.279	−0.297	−0.273
C6–C7	ρ	0.282	0.300	0.297	0.293	0.300
	$\nabla^2\rho$	−0.695	−0.796	−0.777	−0.749	−0.790
	$G(r)$	0.082	0.090	0.088	0.087	0.091
	$H(r)$	−0.256	−0.289	−0.282	−0.274	−0.288
C7–C8	ρ	0.291	0.301	0.303	0.303	0.299
	$\nabla^2\rho$	−0.723	−0.805	−0.800	−0.789	−0.786
	$G(r)$	0.091	0.0917	0.094	0.097	0.098
	$H(r)$	−0.272	−0.293	−0.294	−0.294	−0.295
C8–C9	ρ	0.290	0.284	0.299	0.299	0.300
	$\nabla^2\rho$	−0.734	−0.740	−0.795	−0.786	−0.790
	$G(r)$	0.088	0.076	0.290	0.092	0.080
	$H(r)$	−0.272	−0.262	−0.489	−0.288	−0.276
C9–C4	ρ	0.276	0.319	0.300	0.296	0.295
	$\nabla^2\rho$	−0.661	−0.863	−0.777	−0.766	−0.758
	$G(r)$	0.078	0.108	0.092	0.088	0.086
	$H(r)$	−0.244	−0.323	−0.286	−0.280	−0.276
C9–N1	ρ	0.306	0.275	0.289	0.298	0.300
	$\nabla^2\rho$	−0.736	−0.814	−0.816	−0.788	−0.843
	$G(r)$	0.296	0.148	0.215	0.254	0.240
	$H(r)$	−0.480	−0.351	−0.419	−0.451	−0.450

(Continued)

TABLE X
(Continued)

		Indole			Methyl–indole	
X		—	Al	Mg (3*c*)	—	Mg (3*c*)
C3–C10	ρ	—	—	—	0.248	0.241
	$\nabla^2\rho$	—	—	—	−0.573	−0.535
	$G(r)$	—	—	—	0.057	0.058
	$H(r)$	—	—	—	−0.200	−0.192
X–N1	ρ	—	—	—	—	—
	$\nabla^2\rho$	—	—	—	—	—
	$G(r)$	—	—	—	—	—
	$H(r)$	—	—	—	—	—
X–C2	ρ	—	—	—	—	—
	$\nabla^2\rho$	—	—	—	—	—
	$G(r)$	—	—	—	—	—
	$H(r)$	—	—	—	—	—
X–C3	ρ	—	0.068	0.038	—	—
	$\nabla^2\rho$	—	0.189	0.175	—	—
	$G(r)$	—	0.068	0.042	—	—
	$H(r)$	—	−0.021	0.002	—	—
X–C4	ρ	—	—	—	—	—
	$\nabla^2\rho$	—	—	—	—	—
	$G(r)$	—	—	—	—	—
	$H(r)$	—	—	—	—	
X–C5	ρ	—	0.063	—	—	0.036
	$\nabla^2\rho$	—	0.151	—	—	0.165
	$G(r)$	—	0.058	—	—	0.040
	$H(r)$	—	−0.020	—	—	0.002
X–C6	ρ	—	—	—	—	—
	$\nabla^2\rho$	—	—	—	—	—
	$G(r)$	—	—	—	—	—
	$H(r)$	—	—	—	—	—
X–C7	ρ	—	—	—	—	—
	$\nabla^2\rho$	—	—	—	—	—
	$G(r)$	—	—	—	—	—
	$H(r)$	—	—	—	—	—
X–C8	ρ	—	—	—	—	—
	$\nabla^2\rho$	—	—	—	—	—
	$G(r)$	—	—	—	—	—
	$H(r)$	—	—	—	—	—

For magnesium, besides the complex analogous to **Al–c3**, three more isomers have been located. The global minimum corresponds to the **Mg–Pyr** complex (see Fig. 5), where the magnesium interacts with the benzene ring of the indole. The **Mg–c3** is 9 kcal/mol higher in energy. Two more complexes where the Mg–N interactions are involved have been located, **Mg–c2** and **Mg–c9**, both about 20 kcal/mol higher in energy than the ground state. For the sake of brevity, we will focus our discussion on the comparison between the analogous **X–c3** complexes.

The structural modification undergone by the indole ligand in the **Mg–c3** complex is not as noticeable as that induced by aluminum. The bond length changes are smaller, the planarity is also lost, but the C2–C3–C4–C6 dihedral is only 10°, while it was 23° in the aluminum complex. The Mg–C distances are also larger, all these indicating weaker interactions between Mg and indole.

Bader and NBO analyses of these **X–c3** complexes were also performed. Notice that for magnesium only one bond critical point was located corresponding to Mg–C3, and no bond critical point is found for Mg–C5 nor for Mg–C4 despite having the shortest distance between atoms. NBO describes this complex to be bound due to second order interactions occurring as charge donations from the $\pi_{C2–C3}$ and $\pi_{C5–C6}$ to the magnesium empty out-of-plane *p*-orbital. These donations contribute with 22.68 and 12.71 kcal/mol, respectively. The C–C charge density at the bond critical point vs. the bond length for X–indole is plotted in Figure 6. The indole C–C bonds lie in the region corresponding to the bonds with bond order of 1.5. The aluminum, however, alters substantially the character of the indole C–C bonds. We found one bond in the region of bond order 2, which corresponds to the N–C2 bond, along with four bonds close to the zone corresponding to bonds with order 1, C2–C3, C3–C4, C4–C5, and C5–C6, that is, the carbon atoms which are closer to the aluminum cation. Magnesium also alters the bonding properties of the indole. As for aluminum, a bond order of 2 is observed for N–C2, but only one bond, C3–C4, lies in the one bond order area.

Finally, we have added a methyl to the C3, in order to build an accurate representation of the *Trp* functional group. In this case, no aluminum complexes were found. For magnesium the same complexes as Mg(II)–indole were located. The lowest energy structure also corresponds to the **Mg–pyr** complex, which has a binding energy of 151.63 kcal/mol. **Mg–c3**, **Mg–c2**, and **Mg–c9** are 9, 15, and 18 kcal/mol higher in energy, respectively.

As above, we will only describe the **Mg–c3** complex, which does not differ much from the nonmethylated complex, as can be observed in

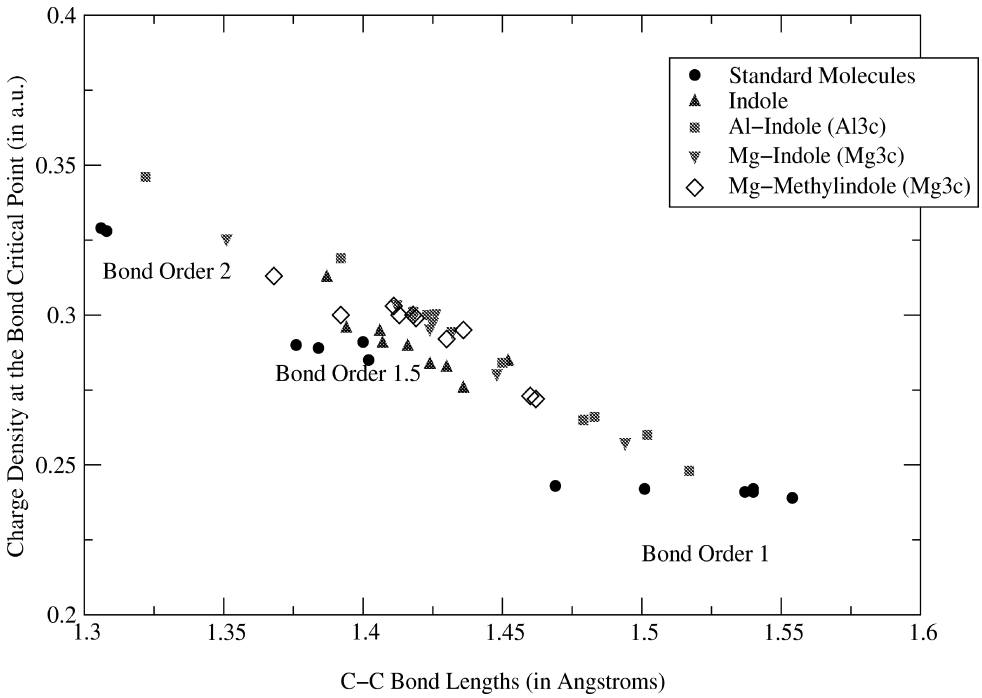

FIGURE 6. Charge densities at the bond critical points are plotted vs. the C–C bond length of the indole (the unfilled triangles) before and after binding to the metal cations (structure X–c3). The squares correspond to aluminum complexes and the triangles to Mg–c3 complexes. These values are compared with some hydrocarbons possessing (according to the Lewis model) known bond orders of 2 (C_2H_4N, C_3H_6O), 1.5 ($C_3H_3^+$, $C_2H_5^+$, . . .), and 1 (C_2H_6, C_4H_6, etc.). Taken from ref. [33].

Table VIII. However, the methyl drives a small displacement in the magnesium cation. In this complex the Mg–C5 is shorter than the Mg–C3. Similarly the NBO charges are nearly unchanged with the exception of the C3 charge, which is 0.084 e^- since the methyl binds to this atom. The Bader analysis, in agreement with the geometrical features, reports that Mg is bound to C5 (by an ionic bond) and not to C3 as it was in the nonmethylated **Mg–c3** complex. This effect may be understood in terms of the electron delocalization pattern induced by the resonances of indole. The C3 is one of the positions where negative charge is concentrated. Thus, when a methyl group binds this position, that resonant form is destabilized, and the magnesium cation prefers to bind C5 instead of C3. A similar explanation could be applied to account for the lack of an **Al–c3** complex. In all the aluminum complexes studied in this work, we have observed that aluminum always interacts with two or more atoms in order to form stable complexes. After methylation C5 is the only binding site for the cation; hence aluminum (III) cannot form a stable complex. Note that in the X–trp complexes described above the ellipticities are not as large as they were in the previous complexes since the bonds involved in the X–c3 complexes are located outside the aromatic rings of the ligand.

Conclusions

We have studied the interactions between the aromatic ring containing aminoacid side chains with the aluminum (III) and magnesium (II) cations. We have characterized several types of complex stable minima on their corresponding potential energy surfaces, namely, complexes in which the metal cation interacts with the aromatic ring, complexes in which the magnesium interacts with the oxygen of the alcohol group of *Tyr*, complexes where the magnesium interacts with the nitrogen of the *Trp*, and finally complexes where the cations interact with three carbons of *Trp* (**X–c3**).

The strongest binding occurs between the aluminum (III) cation and the indole, with a binding energy of 447 kcal/mol, **Al–c3**. For the magnesium (II) the strongest binding among these complexes was in the **Mg–pyr** complex of the methyl–indole, with a binding energy of 151 kcal/mol. *Phe* and *Tyr* have binding energies of 404 and 418 kcal/mol with aluminum and 133 and 136 kcal/mol with magnesium. These binding energies are significantly smaller than the binding energies between these cations and the negatively charged ligands like COO^- or SH^- with binding energies around 740 and 380 kcal/mol for aluminum and magnesium cations, respectively. Aluminum (III) and magnesium (II) interactions with neutral ligands, however, are around 40 kcal/mol for aluminum and around 10 kcal/mol weaker than the interactions with the *Trp* chain.

An important difference between the aluminum (III) and magnesium (II) complexes is that the aromatic ligands lose the aromaticity after binding to the aluminum while the magnesium complexes retain it. This is because the large charge transfer to aluminum removes the electronic density formerly available for delocalization.

This remarkable prediction can be tested by experiment. Namely, it is well known that the out-of-plane skeletal deformations of aromatic compounds lie between 650 and 750 cm^{-1}, and the region around 800 cm^{-1} is blank. However, cyclohexene has out-of-plane vibrations absorbing around 800 cm^{-1}. Indeed, we have found the out-of-plane ring bending of benzene at 678 cm^{-1}, in agreement with the experimental band at 690 cm^{-1}. However, for Al–benzene this band is predicted to shift to 818 cm^{-1}. This might be seen as a clear indication that this vibration mode resembles the out-of-plane ring bending vibration of ciclohexene, where the carbon atoms are singly bonded rather than the out-of-plane ring bending of benzene, and hence this proves that the benzene ring of Al–benzene has lost its aromaticity as a result of the interaction with cation. On the contrary, for the Mg–benzene this band appears at 763 cm^{-1}, which remains in the region of the aromatic out-of-plane skeletal deformation range.

The charge transfer between the cations and the ligand has a maximum in the X–indole complex, where the aluminum cation has a charge of 1.976 e^- and the magnesium cation has a charge of 1.761 e^-. This transfer is not as large as that observed in the sulfur containing aminoacid side chain complexes but is significantly larger than the charge transfer found in the side chains of the acid and acid derivative aminoacids.

The Bader analysis reports covalent bonds between the aluminum and the carbons, and ionic for the magnesium, while the NBO describes the X–C bonds as being due to second order interactions. NBO reports similar interactions between all

the carbons and the metal cation, while the Bader analysis only reports bonds between certain carbons of the aromatic ring. However, the high ellipticities of these bonds together with the similar value of the bond and ring critical point densities indicate that these bonds may collapse easily into different X–C bonds, in agreement with the NBO picture. The Bader analysis also shows in a very elegant way the loss of aromaticity of the benzene rings upon complexation with the aluminum (III) cation.

ACKNOWLEDGMENTS

J.M.M. thanks the Basque Government (Eusko Jaurlaritza) for a grant. Financial support from the Spanish DGICYT and from the Provincial Government of Gipuzkoa (Gipuzkoako Foru Aldundia) is gratefully acknowledged.

References

1. Williams, R. J. P. Coor Chem Rev 1996, 149, 1.
2. Cotton, F. A.; Wilkinson, G. Advanced Inorganic Chemistry; Oxford University Press: New York, 1989.
3. Silva, J. J. R. F. D.; Williams, R. The Biological Chemistry of Elements; Clarendon: Oxford, 1991.
4. Martin, R. B. Clin Chem 1986, 32, 1797.
5. Birchall, J. D.; Exley, C.; Chapell, J. S.; Philips, M. J. Nature (London) 1989, 146–148, 338.
6. Kinraide, T. B.; Parker, D. R. Phys Plant 1990, 79, 283.
7. Parker, D. R.; Bretsch, P. Environ Sci Technol 1992, 26, 908.
8. Bollard, E. G. Involvement of Unusual Elements in Plant Growth and Nutrition in Inorganic Plant Nutrition; Läuchli, A.; Bielski, R. L., Eds.; Springer-Verlag: Berlin, 1983; pp. 659–744.
9. Meri, H.; Banin, E.; Roll, M.; Rousseau, A. Progr Neurobiol 1993, 40, 89.
10. Goyer, R. A. Annu Rev Nutr 1997, 17, 37.
11. Ganrot, P. O. Env Hth Period 1986, 65, 363.
12. Macdonald, T. L.; Martin, R. B. Trends Biochem Sci 1988, 13, 15.
13. Pohlmeier, A.; Knoche, W. Int J Chem Kinetics 1996, 28, 125.
14. Candy, J. M.; McArthur, F. K.; Oakley, A. E.; Taylor, G. A.; Mountfort, C. P. L.; Thompson, J. E.; Beyreuther, P. R. C. H. E. B. K.; Perry, G.; Ward, M. K.; Martyn, C. N.; Edwardson, J. A. J Neurol Sci 1992, 107, 210.
15. Bhattacharyya, M. H.; Wilson, A. K.; Silbergeld, E. K.; Watson, L.; Jeffrey, E. Metal Induced Osteotoxicities; Goyer, R. A.; Klaassen, C. D.; Waalkes, M. P., Eds.; Academic: San Diego, 1995; Vol. 525.
16. Tunega, D.; Haberhauer; Gerzabek, M.; Lischka, H. J Phys Chem A 2000, 104, 6824.
17. Schröder, D.; Schwarz, H. J. J Phys Chem A 1999, 103, 7385.
18. Allen, M. H.; Hutchens, T. W. Rapid Commun Mass Spectrom 1992, 308, 6.
19. Hutchens, T. W.; Allen, M. H. Rapid Commun Mass Spectrom 1992, 469, 6.
20. Garmer, D. R.; Gresh, N. J Am Chem Soc 1994, 116, 3556.
21. Gresh, N.; Stevens, W. J.; Krauss, M. J Comput Chem 1995, 16, 843.
22. Gresh, N.; Garmer, D. R. J Comput Chem 1996, 17, 1481.
23. Deerfield, D. W.; Fox, D. J.; Gordon, M. H.; Hiskey, R. G.; Pedersen, L. G. Proteins Struct Funct Gen 1995, 21, 244.
24. Tortajada, J.; Leon, E.; Morizur, J.-P.; Luna, A.; Mo, O.; Yañez, M. J Phys Chem 1995, 99, 13890.
25. Tortajada, J.; Leon, E.; Luna, A.; Mo, O.; Yañez, M. J Phys Chem 1994, 98, 12919.
26. Luna, A.; Amekraz, B.; Tortajada, J.; Morizur, J. P.; Alcami, M.; Mo, O.; Yañez, M. J Am Chem Soc 1998, 120, 5411.
27. Mercero, J. M.; Fowler, J. E.; Ugalde, J. M. J Phys Chem 1998 102, 7006.
28. Mercero, J. M.; Fowler, J. E.; Ugalde, J. M. J Phys Chem 2000, 104, 7053.
29. Mercero, J. M.; Fowler, J. E.; Irigoras, A.; Lopez, X.; Ugalde, J. M. J Phys Chem, in press.
30. Kumpf, R. G.; Dougherty, D. A. Science 1993, 261, 1708.
31. Ma, J. C.; Dougherty, D. A. Chem Rev 1997, 97, 1303.
32. Sussman, J. L.; Harel, M.; Frolow, F.; Oefner, C.; Goldman, A.; Tolker, L.; Silman, I. Science 1991, 253, 872.
33. Ngola, S.; Dougherty, D. A. J Org Chem 1998, 63, 4566.
34. Ting, A. Y.; Shon, I.; Lucero, C.; Schultz, P. G. J Am Chem Soc 1998, 120, 7135.
35. Zoltewitz, J. A.; Maier, N. M.; Fabian, W. M. F. J Org Chem 1998, 63, 4985.
36. Pandey, R.; Rao, B. K.; Jena, P.; Alvarez-Blanco, M. J Am Chem Soc 2001. Published on the web.
37. Cubero, E.; Luque, F. J.; Orozco, M. Proc Natl Acad Sci USA 1998, 95, 5976.
38. Dumbar, R. C. J Phys Chem A 1998, 102, 8946.
39. Nicholas, J. B.; Hay, B. P.; Dixon, D. A. J Phys Chem A 1999, 103, 1394–1400.
40. Gapeev, A.; Yang, C.-N.; Klippenstein, S. J.; Dumbar, R. C. J Phys Chem A 2000, 104, 3246.
41. Cabarcos, O. M.; Weinheimer, C. J.; Lisy, J. M. J Chem Phys 1999, 110, 8429.
42. Niclaus, M. C.; Neamati, N.; Hong, H.; Mazumder, A.; Sunder, S.; Chem, J.; Milne, G. W. A.; Pommier, Y. J Med Chem 1997, 40, 920.
43. Cubero, E.; Orozco, M.; Luque, F. J. J Phys Chem A 1999, 103, 315.
44. Frisch, M. J., et al. Gaussian 98, A.5.; Gaussian, Inc.: Pittsburgh, PA, 1998.
45. Lee, C.; Yang, W.; Parr, R. G. Phys Rev B 1988, 37, 785.
46. Becke, A. D. J Chem Phys 1993, 98, 5648.
47. Stevens, W. J.; Krauss, M.; Basch, H.; Jasien, P. G. Can J Chem 1992, 70, 612.

48. Reed, A. E.; Curtiss, L. A.; Weinhold, F. Chem Rev 1988, 88, 899.
49. Bader, R. F. W. Atoms in Molecules: A Quantum Theory; Clarendon: Oxford, 1990; Chap. 7.
50. Foster, J.; Weinhold, F. J Am Chem Soc 1980, 102, 7211.
51. Glendening, E. D.; Reed, A. E.; Carpenter, J. E.; Weinhold, F. NBO version 3.1.
52. Biegler-Koning, F. W.; Bader, R. F. W.; Tang, T. H. J Comput Chem 1980, 27, 1924.
53. Schaftenaar, G.; Noordik, J. J Comput-Aided Mol Design 2000, 14, 123.
54. Cioslowski, J.; Mixon, S. T.; Edwards, W. D. J Am Chem Soc 1991, 113, 1083.
55. Dedonder-Lardeux, C.; Grosswasser, D.; Jouvet, C.; Martrenchard, S. Phys Chem Comm 2001, 4.